processes

MDPI

Article

The Effect of Wettability and Flow Rate on Oil Displacement Using Polymer-Coated Silica Nanoparticles: A Microfluidic Study

Mohamed Omran *, Salem Akarri and Ole Torsaeter

Department of Geoscience and Petroleum, Norwegian University of Science and Technology, 7031 Trondheim, Norway; salem.s.f.akarri@ntnu.no (S.A.); ole.torsater@ntnu.no (O.T.)

* Correspondence: mr.mohamed.fathy.omran@gmail.com; Tel.: +47-46217833

Received: 30 July 2020; Accepted: 12 August 2020; Published: 15 August 2020

Abstract: Polymer-coated silica nanoparticles (PSiNPs) have been experimentally investigated in core- and micro-scale studies for enhanced oil recovery (EOR). Wettability and flow rate have a considerable effect on oil displacement in porous media. This work investigates the efficiency of PSiNPs for oil recovery on micro-scale at three wettability states (water-wet, intermediate-wet, and oil-wet). In addition, a cluster mobilization regime is considered in all experiments. A microfluidic approach was utilized to perform flooding experiments with constant experimental settings such as flowrate, pore-structure, initial oil topology, porosity, and permeability. In this study, the wettability of the microfluidic chips was altered to have three states of wettability. Firstly, a micro-scale study (brine-oil-glass system) of each wettability condition effect on flow behavior was conducted via monitoring dynamic changes in the oleic phase. Secondly, the obtained results were used as a basis to understand the changes induced by the PSiNPs while flooding at the same conditions. The experimental data were extracted by means of image processing and analysis at a high spatial and temporal resolution. Low injection rate experiments (corresponding to ~1.26 m/day in reservoir) in a brine-oil-glass system showed that the waterflood invaded with a more stable front with a slower displacement velocity in the water-wet state compared to the other states, which had water channeling through the big pores. As a result, a faster stop of the dynamic changes for the intermediate- and oil-wet state was observed, leading to lower oil recoveries compared to the water-wet state. In a cluster mobilization regime, dynamic changes were noticeable only for the oil-wet condition. For the aforementioned different conditions, PSiNPs improved oil displacement efficiency. The usage of PSiNPs showed a better clusterization efficiency, leading to a higher mobilization, smaller remaining oil clusters, and lower connectivity of the residual oil. The knowledge from this experimental work adds to the understanding of the behavior of polymer-coated silica nanoparticles as a recovery agent at different wettability states and a cluster mobilization regime.

Keywords: nanotechnology; nano-silica; microfluidics; EOR; nanoflooding; wettability alteration

1. Introduction

Bera and Belhaj [1] described nanotechnology as a branch of several fields of engineering, science, and technologies that studies materials at the nanoscale level. Due to its very high efficiency and unique capability, nanotechnology has been widely utilized in many applications in medicine, electronics, and engineering [1]. Nanotechnology has presented crucial solutions for important applications in the oil industry such as enhanced oil recovery (EOR) [2,3], drilling fluids [4], and reservoir stimulation [5].

It is essential to find economic and environmental hydrocarbon-extraction methods for meeting the rapid growth in global energy demand which is anticipated to rise by 50% by 2050 [6].

Nanotechnology has been extensively investigated for EOR on a laboratory scale to explore the effectiveness of nanoparticles (NPs) to unlock the trapped oil after primary and secondary schemes. NPs are used to change the fluid properties to be more efficient with favorable mobility [1,2]. In addition, it affects the fluid-fluid and fluid-rock interactions, leading to a change in wettability, interfacial tension, and chemical adsorption on rock surfaces [3,7–10].

An important property of a porous medium is the wetting condition, affecting the pore-scale flow behavior as well as trapping mechanisms. A micro-scale study indicated that the wetting state of the porous medium has an effect on the amount of trapped oil, which was in the form of ganglia in a water-wet sample, and as thin sheet-like layers in an oil-wet sample [11]. Herring et al. [12] experimentally showed that different wettability states yield to clearly different flow behaviors: the non-wetting phase invaded the medium with a fingering-type regime in a weakly water-wet system, whereas it invaded with a relatively stable displacement pattern in an intermediate-wet system. Zhao et al. [13] experimentally observed that the injected fluid displaces the defending fluid with a more compact pattern as the ability of displacing fluid to maintain contact with medium increases. In addition, the wetting property of a medium is alterable, consequently affecting displacement mechanisms, for example, via low-salinity waterflooding [14,15] and flooding via polymeric NPs [10].

During the displacement, the displaced fluid is subjected to breaking at different locations of the medium, leaving disconnected components known as clusters (i.e., oil ganglia, blobs, or droplets). The mobilization of these clusters can be achieved by stepwise increases in the injection flowrate due to increasing the pressure across the clusters as the driving force for rupturing. Zarikos et al. [16] showed that with an adequate increase in flow rate, parts of ganglia rupture to be mobilized, blobs likely to be mobilized as a whole, and droplets are less likely to be mobilized. The mobilization is attributed to the increase in the drag force and the pressure of the wetting phase exerted on the fluid-fluid interfaces [16]. Considerable rupture of a ganglion requires a high increase in flowrate to overcome a capillary number threshold value [17]. Zhang et al. [10] brine flooding experiments in a bead pack showed that the trapped oil (trapped due to a capillary number of 10^{-7}) was unlocked due to the increase in the flow rate, leading to incremental recovery of 9.1% and 12.3% of IOIP due to a capillary number of 10^{-5} and 10^{-4}, respectively.

The architecture of the porous system, i.e., the spatial arrangement of the pore bodies and size distribution within the system, affects the porous media capability to trap the defending fluid [18–20]. The snap-off mechanism to trap a fluid with a porous medium is significant to pore-scale displacement events [19]. The aspect ratio between a pore body radius to the throat body radius is considerably related to the occurrence of snap-off events. The medium trapping efficiency declines as the aspect ratio decreases [18,21]. Mahmud and Nguyen [21] found that small aspect ratios limited the snap-off events, resulting in less trapping of the defending phase. Another factor to consider for the trapping efficiency is the coordination number defined as a number of throats connected to a pore-body [18]. Tanino and Blunt [22] presented that the chance of trapping the defending fluid increases by the increase in the coordination number.

Wardlaw and Yu [20] investigated displacement experiments in glass microchips and showed that there is a relation between the initial defending fluid connectivity and the behavior of the displacement process. Herring et al. [23] characterized the topology (connectivity) of the non-wetting phase and showed that the initial topology impacts the medium trapping competency. In oil displacement experiments, the initialization of the oil saturation is engineered, then the control of the initial connectivity of the oil prior to flooding is vital for precise comparisons between different recovery agents such as nanofluids [24,25].

This work investigates the efficiency of PSiNPs for oil recovery on micro-scale at three wettability states (water-wet, intermediate-wet, and oil-wet) while maintaining the same experimental conditions; flow rate, pore structure, initial oil connectivity, and temperature. In addition, a cluster mobilization regime is considered in all experiments. Similar experiments using the brine without PSiNPs were

performed to understand the displacement behavior under different wettabilities for the used porous medium and to understand the induced changes by PSiNPs.

2. Materials and Methods

2.1. Porous Material: Microfluidic Chips

In this study, microfluidic chips made of borosilicate glass (EOR chips, Micronit Microfluidics, Enschede, The Netherlands) were utilized to perform micro-scale experiments to investigate the effect of wettability and flow rate on flow behavior. All the microfluidic chips used in this work have an identical porous structure, created via isotropic etching. Table 1 lists the microfluidic chip properties and Figure 1 shows an image of the porous medium and pore size distribution.

Table 1. Dimensional and petrophysical properties of the porous medium.

Property	Value
Chip dimensions	45 mm × 15 mm × 1.8 mm
Network dimensions	20 mm × 10 mm × 0.02 mm
Chip pore volume	5.7 µL
Network pore volume	2.3 µL
Chip porosity	57%
Chip permeability	2.5 Darcy
Network permeability [1]	8.3 ± 0.1 Darcy
Average pore size [2]	130 µm
Wettability state	Water-wet

[1] The liquid permeability of the pore-network was estimated by following the semi-experimental method by [26]. [2] The average pore size was determined by the algorithm presented by [27].

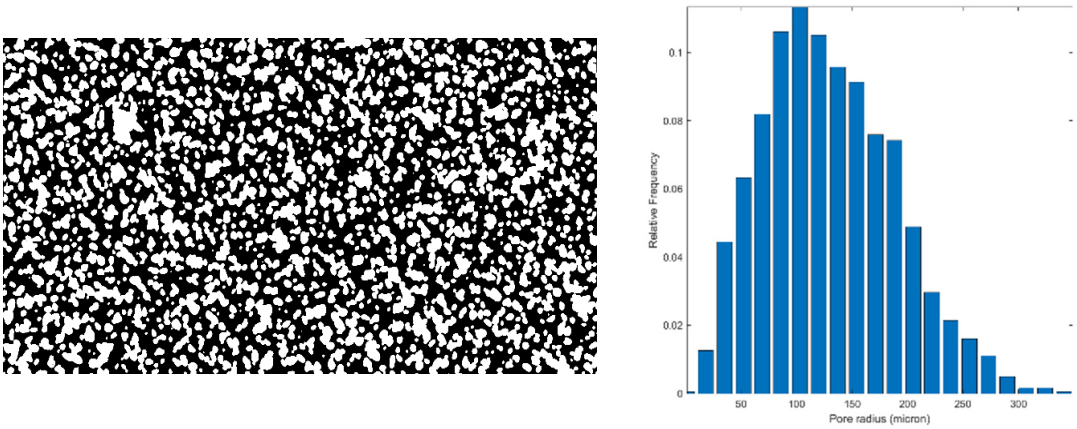

Figure 1. Left: the porous medium (20 mm × 10 mm) contained in the glass microfluidic chip (black: pore space; white: solid phase). **Right**: pore size distribution.

2.2. Fluid Properties

In this study, the oleic phase is dead oil from a field in the North Sea. The displacing fluid is synthetic seawater (SSW), which was also used to prepare a 0.1 wt.% of NPs solution by dilution. Polymer-Coated Silica Nanoparticles were obtained from Evonik Industries (NP20170811-0002-3, Evonik Industries, Hanau, Germany), which were suspended in distilled water at a concentration of 38.6 wt.%. The NPs are hydrophilic with a silica (sol-gel-cationic) basis and surface area in the range of 140–220 m^2/g. Table 2 presents the fluid properties and composition prior to the experiment.

Table 2. Properties and composition of the oil, synthetic seawater, and nanofluid in this study.

Fluid	Property [1]		Oil Composition (%)	
Oil	Density (g/cc)	0.886 ± 0.0002	Saturates	71.57
			Aromatics	20.81
	Viscosity (mPa·s)	34 ± 0.5	Resins	7.44
			Asphaltenes	0.18
Synthetic seawater	Concentration (ppm)	38,318	NaCl	74.40
	Density (g/cc)	1.0243 ± 0.00003	KCl	1.85
	Viscosity (mPa·s)	1.0250 ± 0.0005	$NaHCO_3$	0.57
	pH	7.97 ± 0.002	$NaHCO_3$	10.62
			$CaCl_2.6H_2O$	4.24
	IFT (mN/m)	10.60 ± 0.33	$MgCl_2.6H_2O$	8.25
			$SrCl_2.6H_2O$	0.07
Nanofluid	Suspending agent	Synthetic seawater		
	Concentration of NPs (wt.%)	0.1		
	Density (g/cc)	1.0232 ± 0.00003		
	Viscosity (mPa·s)	1.07 ± 0.003		
	pH	7.85 ± 0.005		
	Size [2] (nm)	32.9 ± 0.376		
	IFT (mN/m)	4.33 ± 0.30		
	NPs basis	Silica (sol-gel-cationic)		
	NPs surface area	140–220 m^2/g		
	NPs wetting state	Hydrophilic NPs		

[1] measured at room temperature (21.5 °C). [2] was determined by dynamic light scattering (DLS) method.

2.3. Experimental Setup

Figure 2 illustrates the microfluidic setup used for the imaging displacement experiments at pore-scale. The main components of the setup are a computer, digital camera (UC90, Olympus, Langhus, Norway), microscope (SZX7, Olympus, Langhus, Norway), flooding holder (Fluidic Connect PRO, Micronit Microfluidics, Enschede, The Netherlands), and syringe pump (33 DDS, Harvard Apparatus, Holliston, MA, USA). Three-way valves were essential for vacuuming, cleaning, and injection. The digital camera acquisition settings are a spatial resolution of 4.6 μm and a temporal resolution of 1 min. The acquisition software was used to capture the images (Stream Basic 2.1, Olympus, Langhus, Norway).

2.4. Experimental Procedures

2.4.1. Contact Angle Measurement

A drop shape analyzer (DSA 100S, Kruss GmbH, Hamburg, Germany) was employed to measure contact angles (a descriptor of wettability) at ambient conditions by using the captive bubble method. Contact angles were measured for two hours (360 measurements), which was enough to obtain measurements with low standard deviations. The bubble was created using a J-shaped needle of a 1.0047 mm inner diameter. The contact angle was measured at three-phase (fluid1-fluid2-solid) contact points by means of image analysis. Fluid1 was either synthetic seawater or nanofluid, fluid2 was oil, and the solid phase was water-wet, intermediate-wet, or oil-wet glass substrate.

2.4.2. Wettability Alteration of Microfluidic Chips

A hydrocarbon-soluble siliconizing fluid (Surfasil TS-42800, Thermo Scientific, Waltham Mass., United States) has been used in literature to modify the porous medium wettability via dilution in a nonpolar organic solvent (i.e., pentene), see Table 3. In this work, Surfasil is diluted in heptane at a concentration of 0.05 and 1 *v*/*v* % to obtain an intermediate- and oil-wet state, respectively. It was found by contact angle measurement on glass substrates that the wettability alteration due to 1 *v*/*v* % is

as effective as 10 *v*/*v* % for the SSW-oil system in this study. A dry and clean microfluidic chip was injected by the solution at an injection rate of 50 µL/min for 10 pore volumes. After that, the microchip was rinsed with the same injection rate by heptane (34873, Sigma-Aldrich, St. Louis, MO, USA) for 50 pore volumes, followed by injecting methanol for 50 pore volumes. The microfluidic chip was heated up at 80 °C for at least 20 min.

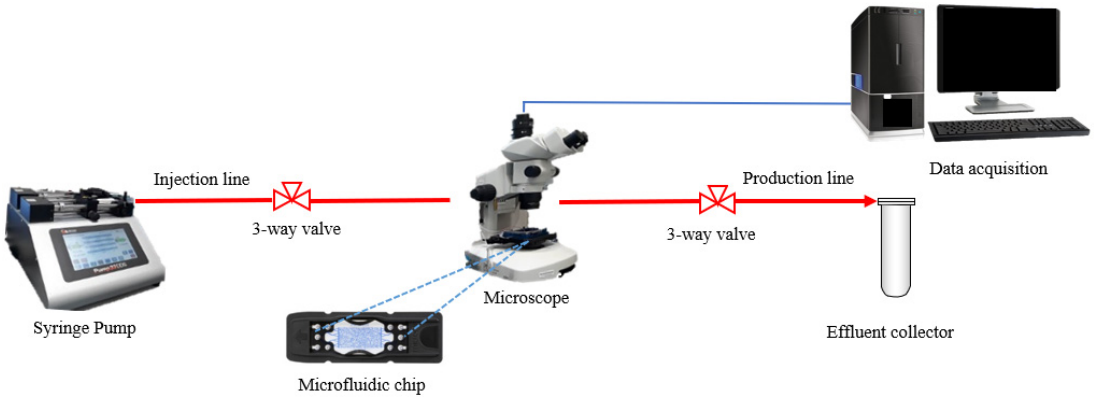

Figure 2. Schematic diagram of the microfluidic setup.

Table 3. Usage of Surfasil in the literature to alter wettability.

Reference	Concentration (*v*/*v* %)	Wettability State
Naderi and Babadgli [28]	Not specified	"Very oil-wet"
Er and Babadgli [29]	10%	"Oil-wet"
Naderi and Babadgli [30]	Not specified	"Strongly oil-wet"
Telmadarreie and Trivedi [31]	10%	144°
Cui and Babadgli [32]	10–15%	125°

2.5. Microfluidic Experiments

An experiment starts by inserting a clean microfluidic chip into the flooding holder. Then, the system is vacuumed to eliminate the air through the production line, while the valve on the injection line is blocked. When the pressure meter of the system shows a value around 60 mbar, the valve is opened to allow the oil to fully saturate the system with an injection rate of 100 µL/min. The injection rate is gradually increased to a maximum value of 200 µL/min to eliminate any residual air bubbles in the system. By this stage, the system is ready to be flooded with SSW or NF at a constant rate using the syringe pump until no more variations are visually detected in the configuration of the oleic phase. During the experiment, dynamic changes in the oil are captured using the digital camera, providing parameters such as oil recovery, oil connectivity, and cluster number. If the objective of the experiment is also to see the flow behavior in a ganglion mobilization regime, the flow rate will be increased by 10 times compared to the previous magnitude. Otherwise, a cleaning process starts with flushing cycles of toluene and methanol until the medium has no oil clusters, then finally flooded by acetone. After cleaning, the chips were heated up at 80 °C for at least 24 h. To the best of our knowledge, there is no standard cleaning method to remove NPs from the porous medium, therefore, microfluidic chips that were exposed to nanomaterials were not reused in this work.

Image Processing and Analysis

Fiji was used to crop the images to remove the holder and boundaries of the microchip and to improve the brightness and contrast between phases via applying a bandpass filter [33]. The images are RGB (red, green, blue) format. The difference between the red and blue (DR-B) for every pixel in the image produced a unique distribution, enabling a tool to distinguish the oil from the other phases (i.e., glass and water). The images were segmented to binary images, whose pixels can have a value of

either zero or one, by selecting a thresholding value from the (DR-B) distribution. By using a MATLAB code (R2019A, MathWorks, Natick, MA, USA), the images were smoothened using a 2-D Gaussian filter and then segmented. Figure 3 illustrates the image processing workflow for a square section (5.62 × 5.62 mm^2) of the microfluidic chip saturated with oil and a rectangular section (13.69 × 10.00 mm^2) saturated with oil and water.

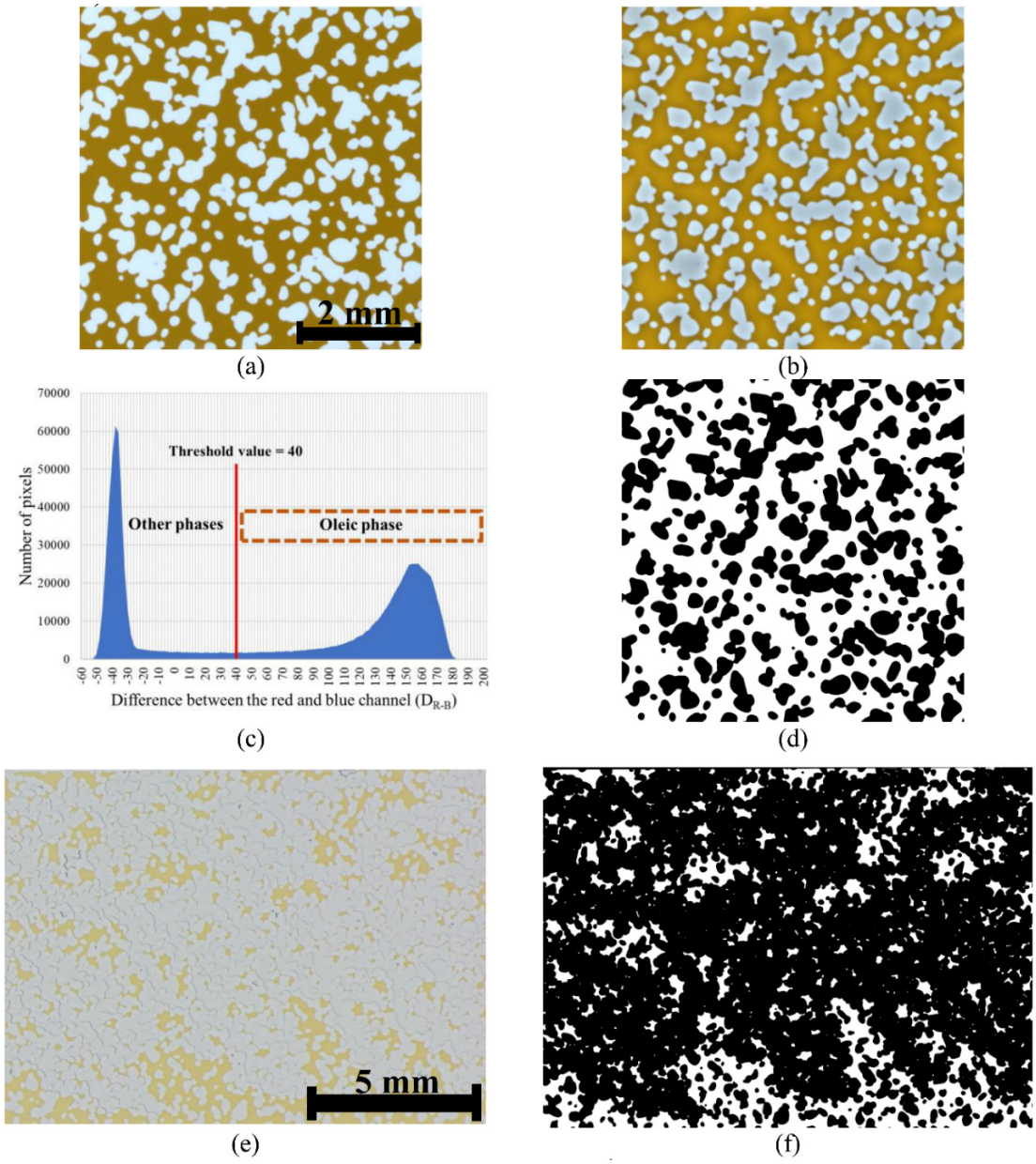

Figure 3. (**a**) a square section (5.62 × 5.62 mm^2) of the microfluidic chip saturated with oil (oil: brown; glass: light color). The workflow for image processing started with filtering the raw image to produce the best brightness and contrast, and to smooth the image. (**b**) the image was filtered with a bandpass filter and a 2-D Gaussian filter to smooth the image. (**c**) (D_{R-B}) distribution of the filtered image is bimodal with the threshold value separating between the oleic phase and glass. (**d**) the image was segmented with the threshold value (oil: white; glass: black). (**e**) a rectangular section (13.69 × 10.00 mm^2) saturated with oil and water (oil: brown; glass and water: light color) and (**f**) the corresponding segmented image (oil: white; glass and water: black).

The code examines the binary images for the number of clusters, oil-connectivity, and sizes of clusters. The gathered data are used to calculate the oil recovery, normalized oil connectivity and cluster number as a function of pore volume injected (PVI). The oil connectivity was determined by Euler number, which is the difference between the number of components (C) in the image and the number of holes (H) within the components/clusters, see Equation (1) [33,34].

$$E = C - H \quad (1)$$

3. Results and Discussion

3.1. Fluid-Solid Interactions

Table 4 presents the contact angles resulting from the interactions between SSW/NF, oil, and glass substrates of different wettability conditions. In this study, the magnitude of change in contact angle of 11.4° and 43.9° for water- and intermediate-wet substrates, respectively, is comparable to reported results in previous work [35–38]. The magnitude of change in the contact angle of 97.55° for an oil-wet substrate with a percent reduction of 66.67%, proves that the used PSiNPs are strongly capable of reducing the oil's ability to maintain contact with an oil-wet medium. The reason for wettability alteration may be attributed to NPs adsorption on the surfaces and disjoining structural pressure [24,39].

Table 4. Fluid-solid interactions indicated by contact angles.

System	Contact Angle (Degree)	% Change in CA [1]
SSW-oil-glass (water-wet)	44.52° ± 0.06°	−25.02%
NF-oil-glass (water-wet)	33.38° ± 0.13°	
SSW-oil-glass (intermediate-wet)	91.30° ± 0.01°	−48.08%
NF-oil-glass (intermediate-wet)	47.40° ± 0.06°	
SSW-oil-glass (oil-wet)	146.30° ± 0.01°	−66.67%
NF-oil-glass (oil-wet)	48.75° ± 0.06°	

[1] compared to the value measured for the SSW-oil system.

3.2. Wettability Effect on Trapping

Three experiments were performed to displace oil by SSW, using water-, intermediate- and oil-wet microfluidic chips, with stepwise increases in the flow rate (0.1 µL/min, 1 µL/min, and 10 µL/min). The flow rate was changed to a higher rate when there were no dynamic changes in the oil configuration within the porous medium.

For the flow rate of 0.1 µL/min (corresponding to ~14.62 µm/s equivalent to 1.26 m/day in reservoir), Figure 4 shows the oil recovery, cluster number, oil connectivity as a function of pore volumes injected, and the residual oil cluster size distribution. The oil recovery was 80.5%, 76.0%, and 74.0% of IOIP for water-wet, intermediate-wet, and oil-wet medium, respectively. The change in wettability in the direction towards the oil-wet state decreased the interval over which the dynamic changes occurred. The changes stopped after 10.4, 2.8, and 1 pore volume injected for water-wet, intermediate-wet, and oil-wet medium, respectively. The intermediate-wet system produced less residual oil clusters with bigger sizes, and less disconnectedness in the oil compared with the water- and oil-wet systems, whereas the water-wet system produced the smallest clusters.

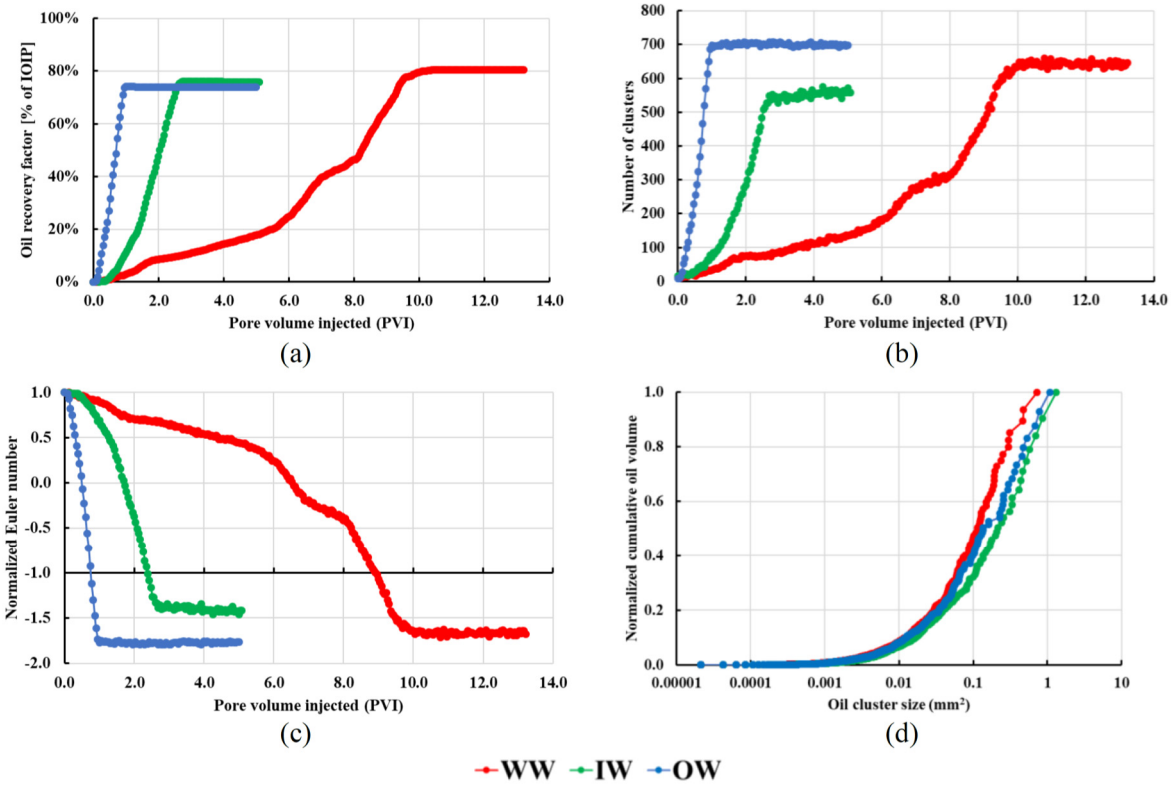

Figure 4. Results for SSW flooding at different wettability states with 0.1 μL/min. Dynamic change in (**a**) oil recovery (**b**) cluster number, (**c**) oil connectivity as a function of pore volumes injected, and (**d**) the residual oil cluster size distribution.

For the water-wet medium, Figure 5 shows that the brine has a better displacement pattern of the oil from the left to the right of the microchip with no further invasion of the unswept areas behind the displacement front. The displacement left the oil trapped by water in the large pores while the brine resided in the small corners and regions. In the oil-wet microchip, the brine was invading the system through the easiest paths, with larger pore- and throat-bodies, leading to less stable displacement pattern, and leaving large oil components in the chip. In other words, the threshold capillary pressure to pass the small regions is higher with the increase of oil wetness. Behind the displacement front, the brine was invading new regions as the number of pore volume injected increased, see the red circles and yellow boxes in Figure 5. The intermediate-wet medium showed less of a stable displacement pattern, as with the behavior in the oil-wet chip, but there was no invasion of the unswept areas behind the front.

The stepwise increases in flowrate showed no effect in the water- and intermediate-wet models. For the oil-wet microchip, the increase from 0.1 to 1 μL/min resulted in no changes, but 10 μL/min mobilized the oil, leading to an incremental recovery of 4.13% and left smaller residual oil clusters in the medium, see Figure 6. The model has a high porosity and permeability which might be the reason that the ultimate recovery of the oil was reached at the lowest rate in the water- and intermediate-wet model, however, the oil-wet model had a higher remaining amount of oil, making it responsive to the high rate. It indicates that an adequate increase in pressure was needed to displace the oil from uninvaded small pore spaces of the oil-wet medium.

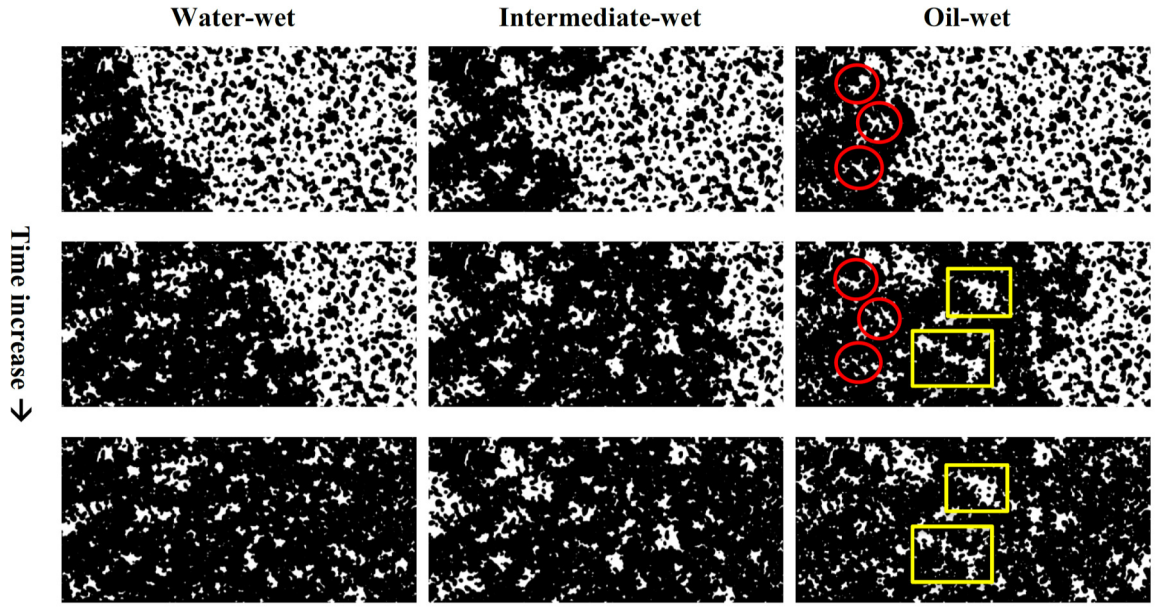

Figure 5. Displacement of the oil by the brine (oil: white; glass and water: black); red circles and yellow boxes show the changes in the oil due to invasion of the unswept areas behind the displacement front, which was only a feature of the oil-wet medium.

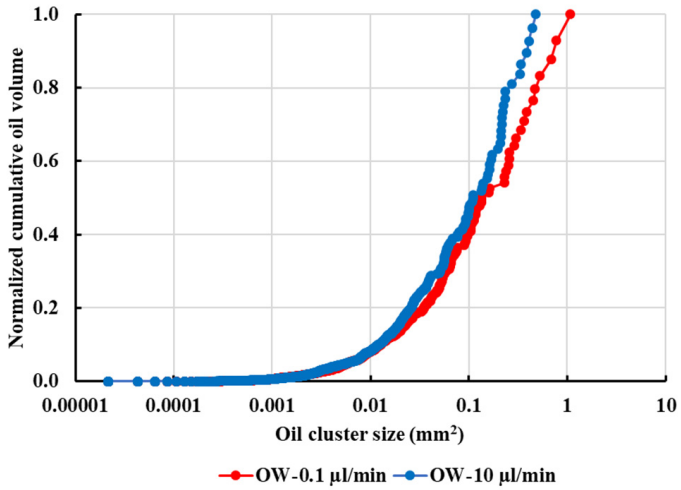

Figure 6. Response in cluster size distribution due to increasing the flow rate of SSW injection from 0.1 µL/min to 10 µL/min. Note: There was no change due to the increase from 0.1 µL/min to 1 µL/min.

3.3. Displacement Via PSiNPs

The flooding with PSiNPs improved the oil recovery performance for the three wetting conditions, in addition to reducing the pore volume injected to reach the ultimate oil recovery, see Figure 7. The nanoflooding has a better mechanism of disconnecting the oleic phase, comparing Figure 4c to Figure 8a, and reducing the cluster sizes, comparing Figure 4d to Figure 8b. Figure 7 shows that the performance of the PSiNPs was better in the water-wet and oil-wet system compared to the intermediate-wet. However, the intermediate-wet had smaller clusters compared to the oil-wet medium, see Figure 8b. Behind the displacement front in the oil-wet chip, the brine was invading new regions as the number of pore volume injected increased, however, it was inconsiderable compared to the flooding without PSiNPs. This can be due to the improved invasion of the small pore regions due to the reduction in contact angle as previously shown. In the water-wet chip, there was an improvement in the displacement pattern due to the usage of PSiNPs, see Figure 9.

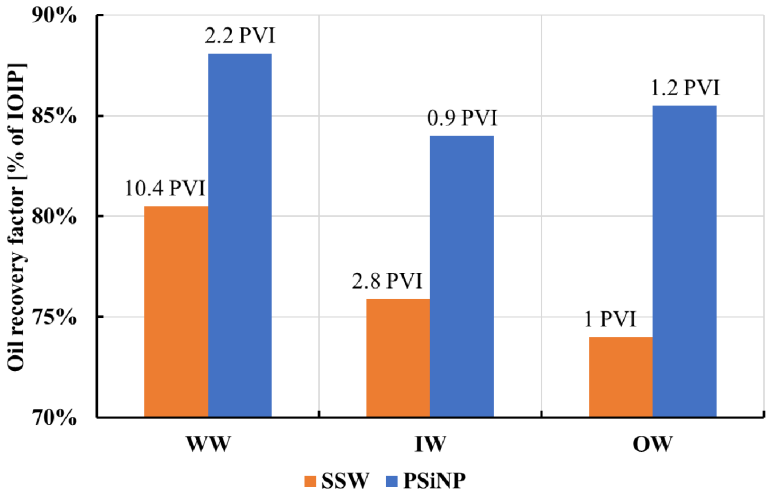

Figure 7. Ultimate oil recovery and corresponding injected pore volume (PVI) for SSW and PSiNP flooding at 0.1 μL/min.

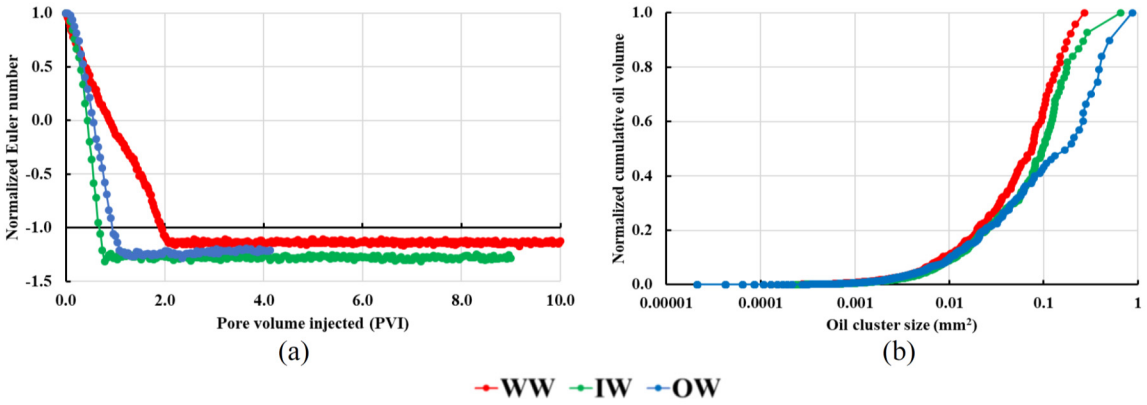

Figure 8. Results for PSiNPs flooding at different wettability states with 0.1 μL/min. Dynamic change in (**a**) oil connectivity as a function of pore volumes injected, and (**b**) the residual oil cluster size distribution.

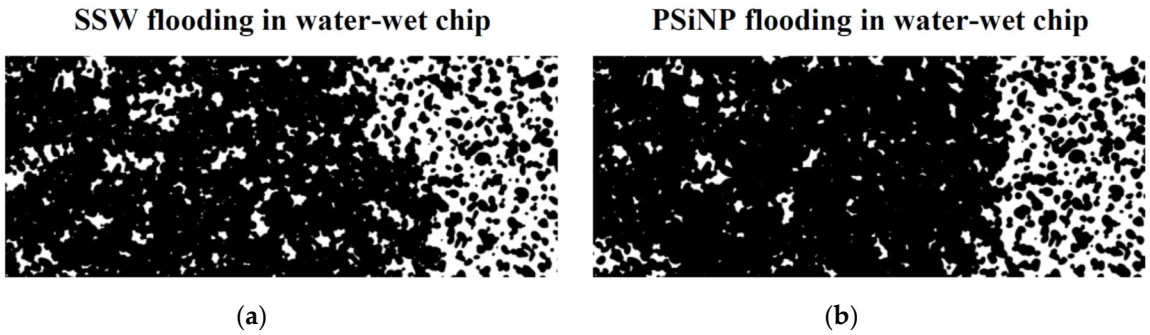

Figure 9. Displacement of the oil by the SSW (**a**) and PSiNPs (**b**) (oil: white; glass and water: black).

Similar to the SSW flooding, there was no response to increasing the flow rate to 1 μL/min and 10 μL/min in the water- and intermediate-wet system. However, the oil-wet medium had smaller clusters and an improvement in oil recovery with the stepwise increases in flow rate, see Figure 10. The recovery mechanism by PSiNPs is credited to the wettability alteration, nanoparticle adsorption, IFT reduction, and small particle sizes.

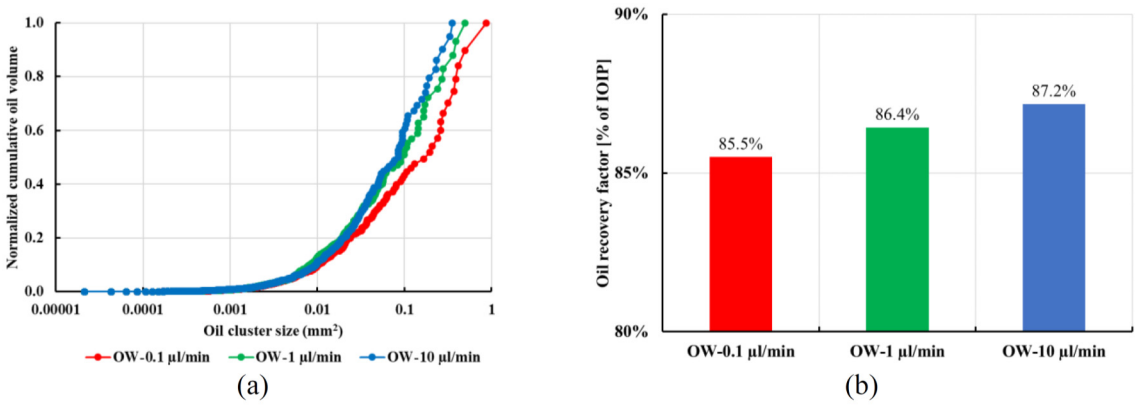

Figure 10. Response in (**a**) cluster size distribution and (**b**) oil recovery due to increasing the flow rate of PSiNPs flooding from 0.1 µL/min to 1 µL/min and then to 10 µL/min.

4. Conclusions

The following conclusions can be drawn based on the work performed on micro-scale for investigating the efficiency of polymer-coated silica nanoparticles (PSiNPs) for oil recovery on micro-scale at three wettability states (water-wet, intermediate-wet, and oil-wet). In addition, a cluster mobilization regime is considered in all experiments:

- A hydrocarbon-soluble siliconizing fluid can successfully generate glass substrates and microfluidic chips of different wettability conditions via controlling the concentration, as proved by contact angle measurement on glass substrates and dynamic flow behavior in the microfluidic chips.
- Polymer-coated silica nanoparticles considerably changed the magnitude of contact angle in water-, intermediate- and oil-wet substrates by 11.4°, 43.9°, and 97.55°, respectively.
- The oil recovery due to SSW flooding was 80.5%, 76.0%, and 74.0% of IOIP for water-wet, intermediate-wet, and oil-wet medium, respectively. However, nanoflooding improved the performance to 88.1%, 84.0%, and 85.5% of IOIP for water-wet, intermediate-wet, and oil-wet chips, respectively.
- The recovery mechanism by PSiNPs is credited to the wettability alteration, nanoparticle adsorption, IFT reduction, and small particle sizes.
- The medium wettability condition controls the displacement invasion pattern, invasion of unswept regions behind the displacement front, and mobilization of trapped clusters by stepwise increases in flowrate.

Therefore, this paper presents some important solutions to the issues researchers have been dealing with to enhance oil recovery. The results of this paper are bringing some useful information that can be used in EOR researches. In addition, the paper presents a systematic study on the mobilization regimes of oil in a porous medium, with emphasis on the effect of polymer-coated silica nanoparticles.

Author Contributions: Conceptualization, M.O.; Funding acquisition, O.T.; Methodology, M.O. and S.A.; Supervision, O.T.; Visualization, M.O. and S.A.; Digital analysis, M.O. and S.A.; Writing—original draft, M.O. and S.A.; Writing—review & editing, S.A. and O.T. All authors have read and agreed to the published version of the manuscript.

Funding: This project is funded by PoreLab Center of Excellence (Grant number 262644), Department of Geoscience and Petroleum, Norwegian University of Science and Technology.

Acknowledgments: This project is supported by PoreLab Center of Excellence, Department of Geoscience and Petroleum, Norwegian University of Science and Technology.

Conflicts of Interest: The authors declare no conflict of interest.

Nomenclature

C	Number of isolated components in an image
CA	Contact angle
E	Euler number
EOR	Enhanced Oil Recovery
H	Number of holes with a component in an image
IFT	Interfacial tension
IOIP	Initial oil in place
IW	Intermediate-wet
NF	Nanofluid
NPs	Nanoparticle
OW	Oil-wet
PSiNPs	Polymer-coated silica nanoparticles
PVI	Pore volume injected
RGB	Red green blue (image format)
sol	Solution
SSW	Synthetic seawater
WW	Water-wet

References

1. Bera, A.; Belhaj, H. Application of nanotechnology by means of nanoparticles and nanodispersions in oil recovery—A comprehensive review. *J. Nat. Gas Sci. Eng.* **2016**, *34*, 1284–1309. [CrossRef]
2. Kamal, M.S.; Adewunmi, A.A.; Sultan, A.S.; Al-Hamad, M.F.; Mehmood, U. Recent Advances in Nanoparticles Enhanced Oil Recovery: Rheology, Interfacial Tension, Oil Recovery, and Wettability Alteration. *J. Nanomater.* **2017**, *2017*, 1–15. [CrossRef]
3. Peng, B.; Zhang, L.; Luo, J.; Wang, P.; Ding, B.; Zeng, M.; Cheng, Z. A review of nanomaterials for nanofluid enhanced oil recovery. *RSC Adv.* **2017**, *7*, 32246–32254. [CrossRef]
4. Rafati, R.; Smith, S.R.; Haddad, A.S.; Novara, R.; Hamidi, H. Effect of nanoparticles on the modifications of drilling fluids properties: A review of recent advances. *J. Pet. Sci. Eng.* **2018**, *161*, 61–76. [CrossRef]
5. Crews, J.B.; Gomaa, A.M. Nanoparticle Associated Surfactant Micellar Fluids: An Alternative to Crosslinked Polymer Systems. In Proceedings of the SPE International Oilfield Nanotechnology Conference and Exhibition, Noordwijk, The Netherlands, 12–14 June 2012. [CrossRef]
6. U.S. Energy Information Administration—EIA. Independent Statistics and Analysis. 2019. Available online: https://www.eia.gov/outlooks/ieo/ (accessed on 11 August 2020).
7. Maghzi, A.; Mohammadi, S.; Ghazanfari, M.H.; Kharrat, R.; Masihi, M. Monitoring wettability alteration by silica nanoparticles during water flooding to heavy oils in five-spot systems: A pore-level investigation. *Exp. Therm. Fluid Sci.* **2012**, *40*, 168–176. [CrossRef]
8. Hendraningrat, L.; Torsæter, O. Understanding Fluid-Fluid and Fluid-Rock Interactions in the Presence of Hydrophilic Nanoparticles at Various Conditions. In Proceedings of the SPE Asia Pacific Oil & Gas Conference and Exhibition, Adelaide, Australia, 14–16 October 2014. [CrossRef]
9. Li, S.; Torsaeter, O. The Impact of Nanoparticles Adsorption and Transport on Wettability Alteration of Intermediate Wet Berea Sandstone. In Proceedings of the SPE Middle East Unconventional Resources Conference and Exhibition, Muscat, Oman, 26–28 January 2015. [CrossRef]
10. Zhang, H.; Ramakrishnan, T.S.; Nikolov, A.; Wasan, D. Enhanced Oil Recovery Driven by Nanofilm Structural Disjoining Pressure: Flooding Experiments and Microvisualization. *Energy Fuels* **2016**, *30*, 2771–2779. [CrossRef]
11. Alhammadi, A.M.; Alratrout, A.; Scanziani, A.; Bijeljic, B.; Blunt, M.J. In situ characterization of mixed-wettability in a reservoir rock at subsurface conditions. *Sci. Rep.* **2017**, *7*, 10753. [CrossRef]
12. Herring, A.; Sheppard, A.; Andersson, L.; Wildenschild, D. Impact of wettability alteration on 3D nonwetting phase trapping and transport. *Int. J. Greenh. Gas Control.* **2016**, *46*, 175–186. [CrossRef]
13. Zhao, B.; MacMinn, C.; Juanes, R. Wettability control on multiphase flow in patterned microfluidics. *Proc. Natl. Acad. Sci. USA* **2016**, *113*, 10251–10256. [CrossRef] [PubMed]

14. Khishvand, M.; Alizadeh, A.H.; Kohshour, I.O.; Piri, M.; Prasad, R.S. In situ characterization of wettability alteration and displacement mechanisms governing recovery enhancement due to low-salinity waterflooding. *Water Resour. Res.* **2017**, *53*, 4427–4443. [CrossRef]
15. Aziz, R.; Niasar, V.; Ferrer, P.J.M.; Godinez-Brizuela, O.E.; Theodoropoulos, C.; Mahani, H. Novel insights into pore-scale dynamics of wettability alteration during low salinity waterflooding. *Sci. Rep.* **2019**, *9*, 1–13. [CrossRef] [PubMed]
16. Zarikos, I.; Terzis, A.; Hassanizadeh, S.M.; Weigand, B. Velocity distributions in trapped and mobilized non-wetting phase ganglia in porous media. *Sci. Rep.* **2018**, *8*, 13228. [CrossRef] [PubMed]
17. Datta, S.S.; Ramakrishnan, T.S.; Weitz, D.A. Mobilization of a trapped non-wetting fluid from a three-dimensional porous medium. *Phys. Fluids* **2014**, *26*, 022002. [CrossRef]
18. Herring, A.; Robins, V.; Sheppard, A.P. Topological Persistence for Relating Microstructure and Capillary Fluid Trapping in Sandstones. *Water Resour. Res.* **2019**, *55*, 555–573. [CrossRef]
19. Blunt, M.J. *Multiphase Flow in Permeable Media: A Pore-Scale Perspective*; Cambridge University Press: Cambridge, UK, 2017.
20. Wardlaw, N.C.; Yu, L. Fluid topology, pore size and aspect ratio during imbibition. *Transp. Porous Media* **1988**, *3*, 17–34. [CrossRef]
21. Mahmud, W.M.; Nguyen, V.H. Effects of Snap-Off in Imbibition in Porous Media with Different Spatial Correlations. *Transp. Porous Media* **2006**, *64*, 279–300. [CrossRef]
22. Tanino, Y.; Blunt, M.J. Capillary trapping in sandstones and carbonates: Dependence on pore structure. *Water Resour. Res.* **2012**, *48*. [CrossRef]
23. Herring, A.; Harper, E.J.; Andersson, L.; Sheppard, A.P.; Bay, B.K.; Wildenschild, D. Effect of fluid topology on residual nonwetting phase trapping: Implications for geologic CO2 sequestration. *Adv. Water Resour.* **2013**, *62*, 47–58. [CrossRef]
24. Omran, M.; Omran, H.; Torsaeter, O. Investigation of the Ionic Interactions of Using Nanoparticles in Waterflooding. In Proceedings of the SPE Europec Featured at 82nd EAGE Conference and Exhibition, Amsterdam, The Netherlands, 8–11 December 2020. [CrossRef]
25. Omran, M.; Akarri, S.; Bila, A.; Torseater, O. Screening of nanoparticles with considering the pore structure and initial oil connectivity effects. In *Paper SPE- 200729-MS, Proceedings of SPE Norway Subsurface Conference, Bergen, Norway, 14 September 2020*; SPE: Richardson, TX, USA, 2020.
26. Pradhan, S.; Shaik, I.; Lagraauw, R.; Bikkina, P. A semi-experimental procedure for the estimation of permeability of microfluidic pore network. *MethodsX* **2019**, *6*, 704–713. [CrossRef]
27. Rabbani, A.; Jamshidi, S.; Salehi, S. An automated simple algorithm for realistic pore network extraction from micro-tomography images. *J. Pet. Sci. Eng.* **2014**, *123*, 164–171. [CrossRef]
28. Naderi, K.; Babadagli, T. Clarifications on Oil/Heavy Oil Recovery Under Ultrasonic Radiation Through Core and 2D Visualization Experiments. *J. Can. Pet. Technol.* **2008**, *47*. [CrossRef]
29. Er, V.; Babadagli, T.; Xu, Z. Pore-Scale Investigation of the Matrix−Fracture Interaction During CO2Injection in Naturally Fractured Oil Reservoirs. *Energy Fuels* **2010**, *24*, 1421–1430. [CrossRef]
30. Naderi, K.; Babadagli, T. Pore-scale investigation of immiscible displacement process in porous media under high-frequency sound waves. *J. Fluid Mech.* **2011**, *680*, 336–360. [CrossRef]
31. Telmadarreie, A.; Trivedi, J.J. New Insight on Carbonate-Heavy-Oil Recovery: Pore-Scale Mechanisms of Post-Solvent Carbon Dioxide Foam/Polymer-Enhanced-Foam Flooding. *SPE J.* **2016**, *21*, 1655–1668. [CrossRef]
32. Cui, J.; Babadagli, T. Retrieval of solvent injected during heavy-oil recovery: Pore scale micromodel experiments at variable temperature conditions. *Int. J. Heat Mass Transf.* **2017**, *112*, 837–849. [CrossRef]
33. Schindelin, J.; Arganda-Carreras, I.; Frise, E.; Kaynig, V.; Longair, M.; Pietzsch, T.; Schmid, B. Fiji: An open-source platform for biological-image analysis. *Nat. Methods* **2012**, *9*, 676–682. Available online: https://imagej.net/Fiji (accessed on 11 August 2020). [CrossRef]
34. Toriwaki, J.; Yoshida, H. *Fundamentals of Three-Dimensional Digital Image Processing*; Springer: Berlin, Germany, 2009.
35. Sivanesapillai, R.; Steeb, H. Fluid Interfaces during Viscous-Dominated Primary Drainage in 2D Micromodels Using Pore-Scale SPH Simulations. *Geofluids* **2018**, *2018*, 1–13. [CrossRef]
36. Metin, C.O.; Baran, J.R.; Nguyen, Q. Adsorption of surface functionalized silica nanoparticles onto mineral surfaces and decane/water interface. *J. Nanopart. Res.* **2012**, *14*, 1–16. [CrossRef]

37. Karimi, A.; Fakhroueian, Z.; Bahramian, A.; Pour Khiabani, N.; Darabad, J.B.; Azin, R.; Arya, S. Wettability Alteration in Carbonates using Zirconium Oxide Nanofluids: EOR Implications. *Energy Fuels* **2012**, *26*, 1028–1036. [CrossRef]
38. Hendraningrat, L.; Li, S.; Torsater, O. Effect of Some Parameters Influencing Enhanced Oil Recovery Process using Silica Nanoparticles: An Experimental Investigation. In Proceedings of the SPE Reservoir Characterization and Simulation Conference and Exhibition, Abu Dhabi, UAE, 16–18 September 2013. [CrossRef]
39. Hu, Z.; Azmi, S.M.; Raza, G.; Glover, P.W.J.; Wen, D. Nanoparticle-Assisted Water-Flooding in Berea Sandstones. *Energy Fuels* **2016**, *30*, 2791–2804. [CrossRef]